ACS NANO
Cite This: ACS Nano 2019, 13, 3931−3939
www.acsnano.org

ARTICLE

Closing the Surface Bandgap in Thin Bi_2Se_3/Graphene Heterostructures

Jimin Chae,[†] Seoung-Hun Kang,[‡] Sang Han Park,[†,§] Hanbum Park,[†] Kwangsik Jeong,[†] Tae Hyeon Kim,[†] Seok-Bo Hong,[†] Keun Su Kim,[†] Young-Kyun Kwon,[‡,∥] Jeong Won Kim,[⊥] and Mann-Ho Cho*[,†]

[†]Department of Physics, Yonsei University, Seoul 03722, Korea
[‡]Korea Institute for Advanced Study, Hoegiro 85, Seoul 02455, Korea
[§]Pohang Accelerator Laboratory, POSTECH, Pohang 790-784, Korea
[∥]Department of Physics and Research Institute for Basic Sciences, Kyung-Hee University, Seoul 02447, Korea
[⊥]Division of Industrial Metrology, Korea Research Institute of Standards and Science, Daejeon 34113, Korea

Supporting Information

ABSTRACT: **Topological insulator (TI), a band insulator with topologically protected edge states, is one of the most interesting materials in the field of condensed matter. Bismuth selenide (Bi_2Se_3) is the most spotlighted three-dimensional TI material; it has a Dirac cone at each top and bottom surface and a relatively wide bandgap. For application, suppression of the bulk effect is crucial, but in ultrathin TI materials, with thicknesses less than 3 QL, the finite size effect works on the linear dispersion of the surface states, so that the surface band has a finite bandgap because of the hybridization between the top and bottom surface states and Rashba splitting, resulting from the structure inversion asymmetry. Here, we studied the gapless top surface Dirac state of strained 3 QL Bi_2Se_3/graphene heterostructures. A strain caused by the graphene layer reduces the bandgap of surface states, and the band bending resulting from the charge transfer at the Bi_2Se_3−graphene interface induces localization of surface states to each top and bottom layer to suppress the overlap of the two surface states. In addition, we verified the independent transport channel of the top surface Dirac state in Bi_2Se_3/graphene heterostructures by measuring the magneto-conductance. Our findings suggest that the strain and the proximity effect in TI/non-TI heterostructures may be feasible ways to engineer the topological surface states beyond the physical and topological thickness limit.**

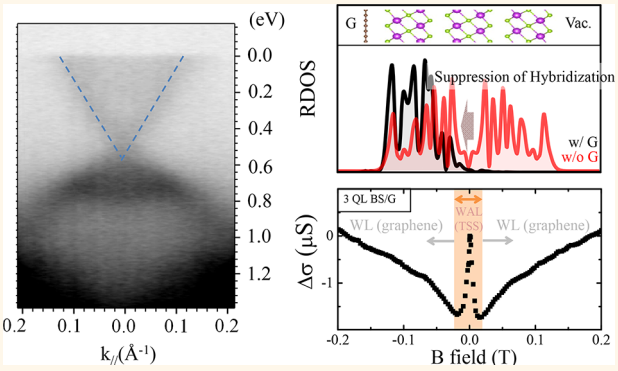

KEYWORDS: *topological insulator, Bi_2Se_3, graphene, heterostructure, strain, band bending, coherence length*

Topological insulator (TI) is one of the most interesting materials in the field of condensed matter physics because it is a bandgap insulator with topologically protected helical edge states.[1,2] Bismuth selenide (Bi_2Se_3) is most spotlighted three-dimensional TI material because it has a metallic single Dirac cone at each surface and a relatively wide bandgap (~0.3 eV), making it suitable for application to low-power electronics and error-tolerant quantum computing, spin devices, and experimental platforms for quantum phenomena.[3,4] To use the surface state of a metallic single Dirac cone, it is necessary to lower the bulk contribution and interference between the Dirac fermions and bulk phonons. Thus, Dirac surface states on few-layer TI films have been studied through both theoretical and experimental approaches.[5,6] Although the surface state is localized at the top- or bottom-most layer in the film, the wave functions are spread over the second or third layer, so that with thicknesses of less than five quintuple layers (QLs) there is an overlap of top and bottom surface states, the so-called "finite-size effect" in TIs. Zhang *et al.*[7] revealed the band gap opening of the Dirac surface band in Bi_2Se_3 films grown by MBE on double-layer graphene with thicknesses less than 3 QLs. Following this experimental finding, an effective model to explain the detailed mechanism of hybridization of surface states was proposed; in the 2D limit, overlap of the wave functions of the top and bottom surface and the structure inversion asymmetry (SIA) from the substrate induce a finite bandgap and Rashba-type spin splitting of the surface Dirac state.[6]

Received: September 13, 2018
Accepted: April 5, 2019
Published: April 5, 2019

DOI: 10.1021/acsnano.8b07012
ACS Nano 2019, 13, 3931−3939

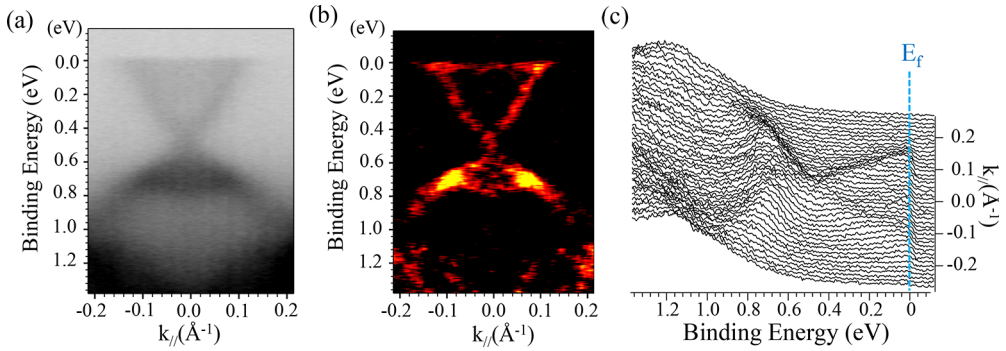

Figure 1. ARPES data for 3 QL Bi_2Se_3 on monolayer graphene/SiC substrate: (a) raw data, (b) second derivative data, (c) EDC curve. Photon energy is 48 eV. A gapless surface state is shown clearly.

Several methods have been proposed to modify the surface states to overcome the physical limits, such as bandgap opening and weakening the topological phase. Applying an electrical potential to the ultrathin film can be a good way to control the surface states and topological phase through modulation of the SIA. The gap control of the surface state of ultrathin TI films with an external electric field was studied experimentally and theoretically by scanning tunneling microscopy and analytic methods.[8,9] In addition, the surface states can be modulated through interaction at the interface without an external field, the so-called "proximity effect". Theoretical studies using density functional theory (DFT) calculations found the possibility of a topological phase transition through band engineering in the heterostructure, consisting of a trivial insulator and nontrivial insulator.[10−12] However, it has been difficult to experimentally verify the modulated topological surface states.

Here, we studied the gapless top surface state of strained 3 QL Bi_2Se_3/graphene heterostructures. Graphene can be a suitable substrate because of its advantages with respect to film growth such as low lattice mismatch with TIs and with respect to transport channels such as good conductance regarding electrons or spin.[5] In particular, based on the reports that the charge transfer between Bi_2Se_3 and graphene occurs within 1 QL of Bi_2Se_3 we can expect much stronger SIA to modulate the surface bands dramatically.[13,14] In the growth systems of Bi_2Se_3/graphene heterostructures, tensile strain in the out-of-plane direction between Bi_2Se_3/graphene can reduce the overlap of the two surface wave functions. In addition, the proximity effect caused by charge transfer at the interface leads to spatial localization of both top and bottom surface wave functions. These effects can reduce the overlap of the two surface states, inducing a closed bandgap for the surface bands. We found a narrow cusp of weak antilocalization (WAL) in the magneto-conductance (MC) of Bi_2Se_3/graphene heterostructures, which implies longer quantum coherence length and a helical surface band structure. In conclusion, we found suppression of the hybridization because of the strain and charge transfer effects from the graphene, resulting in the generation of bandgap closing of the surface band in 3 QL Bi_2Se_3 films.

RESULTS AND DISCUSSION

Hybridization of the two surface states of Bi_2Se_3 films with thicknesses of less than 5 QL was predicted analytically by Shen[6] and observed experimentally using various measurements, such as angle-resolved photoemission spectroscopy[7] (ARPES), terahertz spectroscopy,[15] and transport measurement.[16] In our experiments, we synthesized Bi_2Se_3 films through our specific growth method, varying the film thickness (2−6 QL) on monolayer graphene pregrown on a SiC substrate.[17] The thickness of the samples was confirmed by X-ray reflectivity and AFM measurements, as shown in Supporting Information 1. Similar band structures were observed in relatively thick films (4−6 QL), as shown in Supporting Information 2. Moreover, a small down shift of the Fermi level was apparent with decreasing film thickness. However, the surface band structure of 3 QL Bi_2Se_3 on monolayer graphene abruptly changed from a gap opened structure to a gapless band structure (Figure 1a). The gapless surface of the Dirac cone is observed more clearly in the second-derivative spectrum and energy dispersion curves (EDCs) (Figure 1b,c). The bulk conduction band is not shown in our measurements because of the invalid selection rule with photon energy of 48 eV. The Dirac point of the surface state is located 0.47 eV from the Fermi level, indicating band bending induced by charge transfer between Bi_2Se_3 and graphene. The closed bandgap appears to be somewhat exceptional, considering that the bandgap is reported to be greater than 0.1 eV.

The bandgap opening in the ultrathin film resulted from the hybridization between top and bottom surface states, in which the spatial distribution of two surface bands overlap with each other to form the bandgap in film thickness less than 5 QL. Although there are many experimental reports and theoretical studies about bandgap opening in ultrathin film grown on various substrates,[18−20] some theoretical research has suggested that the spatial distribution and bandgap can be modulated by band bending effects at the interfaces.[10,11] Experimental results of bandgap modulation in ultrathin TI films were also reported. Zhang *et al.* found bandgap modulation of Sb_2Te_3 films with thickness less than 4 QL, which were grown on the $SrTiO_3$ (111) (STO) substrate using low-temperature scanning tunneling microscopy and spectroscopy.[8] They showed the bandgap tunability in each 2, 3, 4 QL Sb_2Te_3 film using the high gating tunability of STO substrate. In addition, they verified the relations between band bending by gating in STO substrate and bandgap modulation through analytic methods. They suggested that the bandgap of the 3 QL Sb_2Te_3 can be closed if the SIA potential exceeds a critical value. After their research, clearer and direct results of bandgap closing in 3 QL Bi_2Se_3 film have been reported. Tsipas *et al.* observed the gapless Dirac cone of high-quality epitaxial Bi_2Se_3 grown on an AlN (0001) substrate using ARPES.[21] They

DOI: 10.1021/acsnano.8b07012
ACS Nano 2019, 13, 3931−3939

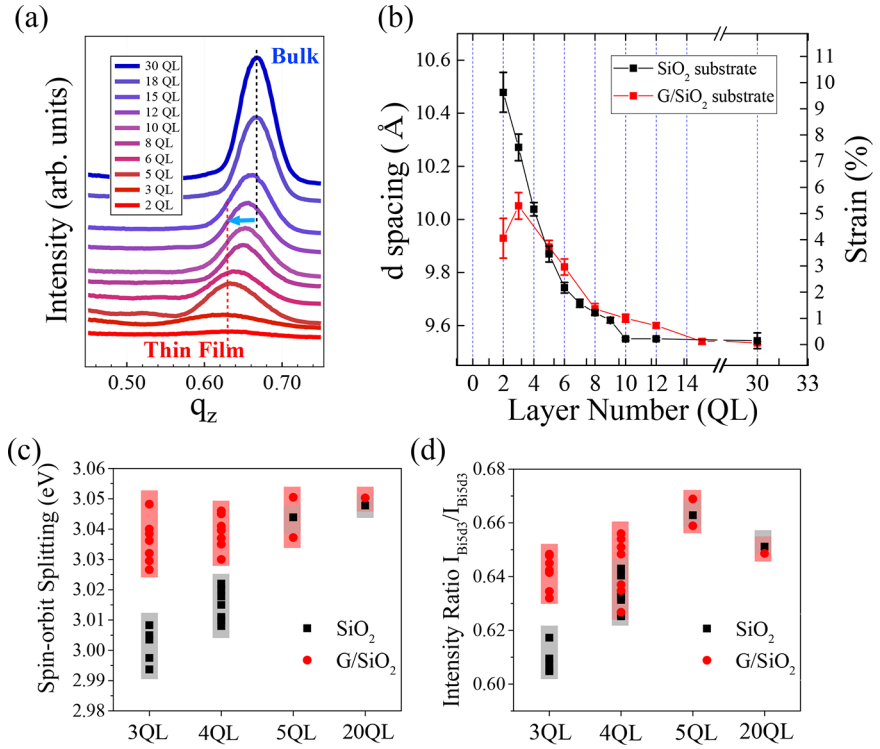

Figure 2. (a) (003) peaks of Bi_2Se_3 films on graphene measured by SAXS and (b) *d*-spacing and strain of Bi_2Se_3 films on graphene and SiO_2 substrate as a function of thickness. In the thin films of 2−3 QL, the Bi_2Se_3 film grown on graphene has a lower strain because graphene has a bigger lattice than Bi_2Se_3. (c) Spin−orbit splitting and (d) intensity ratio between Bi $5d_{5/2}$ and Bi $5d_{3/2}$ as a function of the thickness. With graphene, the spin−orbit splitting and branch ratios do not decrease as the thickness decreases to 3 QL.

suggested that the AlN (0001) substrate allows perfect registry with a minimum reaction and no buffer layer at the interface. The asymmetry between top and bottom surface states suppresses hybridization, resulting in the formation of a gapless Dirac cone. In our experiments, since the monolayer graphene grown on 4H-SiC (0001) is a suitable substrate because of the van der Waals bonding and low lattice mismatch (2.9% tensile strain in the in-plane direction),[22] the Bi_2Se_3 films can be epitaxially grown as high-quality single-crystalline films, without any buffer layer. The 5 QL Bi_2Se_3 films on monolayer graphene show lamellar and 180° in-plane rotational domains, as shown in previous reports of high-quality epitaxial films on AlN,[21] InP, and Si[23] substrates (Supporting Information 3). Thus, the reported data indicate that both high strain and sufficient band bending induce the strong SIA in 3 QL Bi_2Se_3 grown on monolayer graphene/SiC substrate induce bandgap closing.

To verify the experimental evidence for the strain effects, we investigated the strain of Bi_2Se_3 films and the spin−orbit splitting factors of Bi 5d with and without graphene using small-angle X-ray scattering (SAXS) and X-ray photoemission spectroscopy (XPS), respectively. We used the monolayer graphene transferred on SiO_2 substrate. Since detailed parameters and Fermi levels could be slightly different, the structural and electronic influences will be same as SiC substrate (Supporting Information 4). Figure 2a shows the thickness-dependent SAXS pattern of a Bi_2Se_3 film on a graphene substrate. As the film thickness decreases, the position of the main peaks near q = 0.66 Å shifts to a lower value. This confirms our previous results for Bi_2Se_3 film on a SiO_2 substrate without graphene.[24] In case of a SiO_2 substrate without graphene, there is a dramatic increase in the d-spacing value, from 9.542 Å for 30 QL Bi_2Se_3 to 10.478 Å for 2 QL Bi_2Se_3, which results from the typical growth process using a self-ordering growth mechanism during the post annealing process. The strain values of thicker films on the graphene substrates with thicknesses greater than 5 QL are similar to those on SiO_2 substrates. However, the strain values under 5 QL can differ depending on the substrate. The 3 QL Bi_2Se_3 films on graphene/SiO_2 and SiO_2 have strain values of 5.4% and 7.6%, respectively, implying that the tensile strain in the in-plane direction from the graphene contributes to reduction of the tensile strain already generated in the out-of-plane of 3 QL Bi_2Se_3 grown on graphene/SiO_2 substrate. Since the strains of 3 QL Bi_2Se_3 on graphene and SiO_2 substrate are near the topological phase transition region, dramatic changes in band structures can be induced with changes in SOC strength and crystalline properties.[25,26] Interestingly, the strain values of 2 and 3 QL Bi_2Se_3 films on graphene substrates are 4.2% and 5.4%, respectively; the value for the 2 QL film is much lower than that of the 3 QL film, implying that the interfacial strain from the graphene substrate is much more dominant as the thickness decreases within 3 QL.

To verify more detailed effects on the band structure related to the graphene substrate, we measured the spin−orbit splitting of Bi 5d using XPS as a function of Bi_2Se_3 layer thickness on graphene. We could not extract the spin−orbit strength value from the splitting of Bi 5d states because there is no exact formula for the relationship between spin−orbit splitting values and spin−orbit expectation values ⟨L·S⟩ in XPS techniques. Although we could not clarify the exact relationship between the changes of SOC strength due to the strain and bandgap reduction, the changes of SOC strength itself could be a strong factor in the bandgap reduction in these

DOI: 10.1021/acsnano.8b07012
ACS Nano 2019, 13, 3931−3939

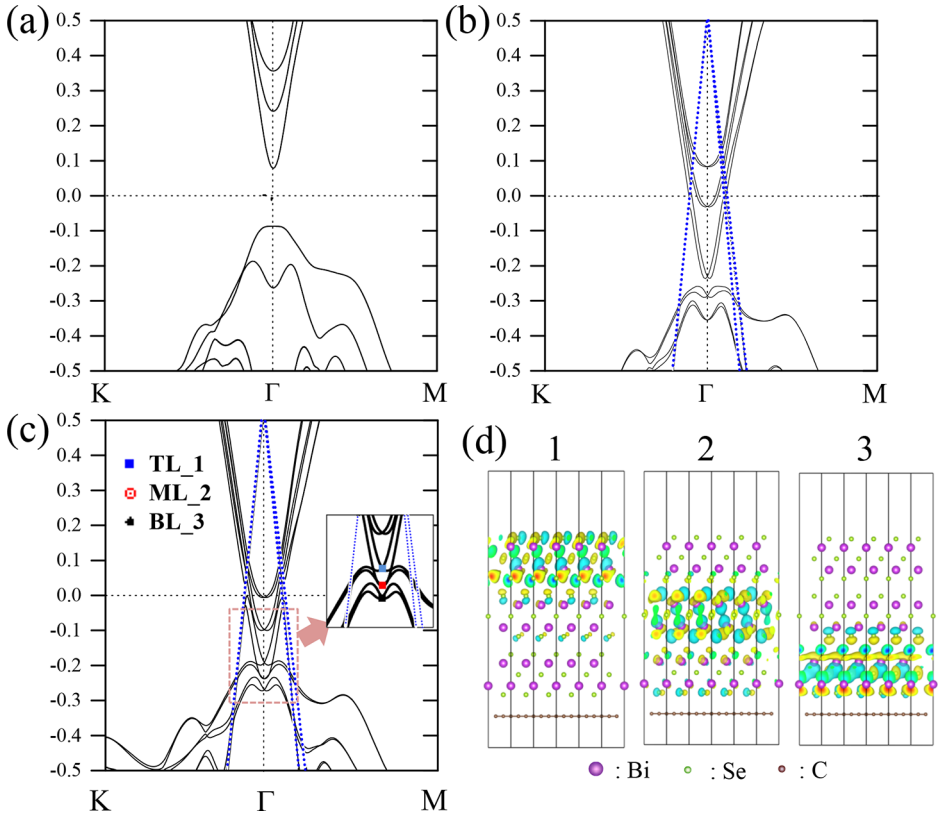

Figure 3. Simulated band structures of (a) bare 3 QL Bi_2Se_3, (b) relaxed 3 QL Bi_2Se_3 with graphene substrate, and (c) strained 3 QL Bi_2Se_3 with graphene substrate. (d) Spatial distributions (yellows and cyan) of the three surface bands in (c) (red and blue are charges that belong to the core part). The graphene has linear bands as represented in (b) and (c) with blue dots. The bandgap of the surface states decreases and was found to be closed with tensile strain in the in-plane direction, followed by the localization of the surface states at each layer.

strain regions of 5−7% in the out-of-plane direction.[25−27] Using fitted data for each peak of Bi $5d_{3/2}$ and $5d_{5/2}$, we plotted the spin−orbit splitting value and spin−orbit intensity ratio, as shown in Figure 2c,d, respectively. No significant difference was observed in the thicker films of 5 QL and 20 QL, which is consistent with the reported cases for bulk Bi_2Se_3.[28] However, although the values of spin−orbit splitting (SOS) and intensity ratio have small variations of 20−30 meV and 0.02−0.03, respectively, in each measurement and each sample split, we can obtain the clear difference in SOS of Bi_2Se_3 films less than 5 QL depending on the substrate that the film is grown on. As the thickness decreases, the film of the SiO_2 substrate shows clear decreases in both SOS as well as intensity ratio. The SOS values of Bi_2Se_3 films on SiO_2 substrates decreases to 3.02 and 3.00 eV for 4 QL and 3 QL, respectively, while those of Bi_2Se_3 films on graphene substrates do not show a meaningful decrease but only some broadening of statistical error. Considering that the strain can modulate the crystal field as well as the SOC, the excess strain in the sample without graphene can induce a decrease in SOS.[25,27] Although the width of the decrease is lower than that of SOS energy, the intensity ratio has a similar tendency with decreasing film thickness in the sample without graphene. This decrease in intensity ratio is related to the crystalline quality. The increase in quality with graphene is reported elsewhere as well as verified by the peak broadness in our SAXS data in Figure 2a.[13,29] Therefore, we conclude that the tensile strain in in-plane direction caused by lattice mismatch with graphene induced the suppression of tensile strain in the out-of-plane direction of 3 QL Bi_2Se_3. Finally, bandgap reduction in Bi_2Se_3 films could be accompanied by the suppression of tensile strain, which is further enhanced by preventing the decrease in spin−orbit coupling and the improved crystal quality of the film grown on the graphene.

To verify the detailed mechanism of bandgap closing for the TSS bands in Bi_2Se_3/graphene heterostructures, we performed an ab initio study for the band structure with and without a graphene layer, as shown in Figure 3. The Fermi level of Bi_2Se_3 shifted upward (bandgap shifted downward and located around −0.25 eV) implying charge transfer with the graphene layer. The clear linear dispersion of the graphene layer in Figure 3b and 3c was found to have its Dirac point at the energy of 0.5 eV (blue dots in Figure 3b). The band gap of Bi_2Se_3 films without graphene layer, as shown in Figure 3 a, was calculated to be 0.18 eV, which is much higher than the reported values of 0.12−0.15 eV.[7,14] When the Bi_2Se_3 is placed on graphene, the bandgap is abruptly reduced to 0.023 eV and the band is changed to Rashba-like dispersion by breaking inversion symmetry, which is consistent with the data reported by other groups.[8,14] In addition to the reduction of the bandgap, there is a change in the spatial distribution of surface states, as shown in Supporting Information 5. The surface bands of conduction bands are localized at the top layer, and the valence bands are at the bottom layer. This localization originates from the band bending effect. Band bending caused by charge transfer at the interface can induce a change in the spatial distribution of surface bands.[10,21] Wu *et al.* studied the locational shift of surface states in the heterostructures of TIs and conventional insulators (ZnM, M = S, Se, Te) in which the direction of the spatial shift to the bulk of TIs or conventional

DOI: 10.1021/acsnano.8b07012
ACS Nano 2019, 13, 3931−3939

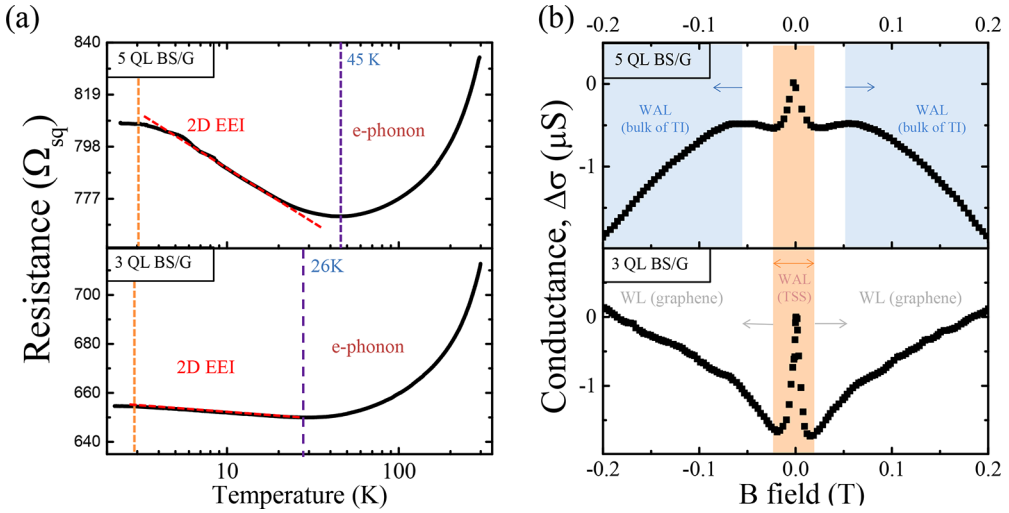

Figure 4. (a) Temperature-dependent resistances of 5 QL (up) and 3 QL Bi_2Se_3 (down) on graphene/SiO_2 substrates. A clear 2D EEI results from the independent transport channels of the Bi_2Se_3 layer and graphene layer. (b) Magneto-conductance curves of 5 QL and 3 QL Bi_2Se_3 on graphene/SiO_2 substrates. There is a narrow cusp of WAL related to the surface states of the TI film. The full-scale and temperature-dependent MC curves are shown in Supporting Information 9.

insulators depends on their band alignment, which is a result of their work functions and bonding nature.[10] Generally, Bi_2Se_3 and graphene have been reported to have work functions of 5 and 4.5 eV, respectively.[30,31] As shown in Supporting Information 6, the work function of our samples was experimentally verified using UPS to be 5.07 and 4.075 eV for Bi_2Se_3 20 nm and graphene on SiC, respectively, indicating that the strong band bending can occur at the interface. The lower work function value of graphene may result from the interaction with the SiC substrate. We determined a work function of 4.75 eV for the 3 QL Bi_2Se_3/graphene heterostructures, which implies that there is a strong band bending. This strong bending induces the spatial shift of surface states to suppress the hybridization of the top and bottom surface.

Although the bandgap decreases considerably for the Bi_2Se_3/graphene heterostructure, in our ARPES data, actually, the surface band has no bandgap and shows a clear linear dispersion, not Rashba-like splitting. Thus, we conclude the another sources should be applied to close the bandgap of TSS and change the detailed parameters in the in-plane directions, considering the SiC substrate we used in ARPES measurements[32] (detailed discussion in Supporting Information 7). We simulated 1% and 2% tensile-strained Bi_2Se_3/graphene heterostructures and found a closed bandgap for the case of 2% tensile strain in the in-plane direction, as shown in Figure 3c. Near the surface band of the Bi_2Se_3 film, there are three states that cross gamma points. These are marked as blue, red, and black dots. We also plotted the spatial distributions of these three bands near the gamma point, as shown in Figure 3d. There is a clear separation of the three bands at the top, middle, and bottom layers of the 3 QL Bi_2Se_3 film. Following the band bending, the lower band belongs to the bottom layer, and there is a closed surface band belonging to the top layer that crosses at the gamma point (Supporting Information 5). These results imply that the two surface states are shifted in the opposite direction following the strong band bending. Finally, the two surface states are localized, suppressing the band hybridization. For the middle layer, there is a hybridized state of the top and bottom surfaces. The mechanisms for the spatial shift and localization of wave functions have been studied by other groups.[33] The wave function of each surface state in bulk or thicker films is well-known to have a decay length of 2 QL.[34] Thus, overlaps between opposite surface states begin to open the surface bandgap when the film thickness decreases below 5 QL. Although the specific values are different from other studies, the 3 QL film has a bandgap of 30−130 meV. In addition, the substrate supporting the film can generate SIA on the TI film, which induces a potential gradient on each surface, so that the surface states at the interface shift upward or downward, followed by the potential.[33,34] For example, when a potassium layer is positioned on top of the Bi_2Se_3 film, the top surface state shifts downward because of the acceptance of electrons from the potassium layer, and each top and bottom surface state shows more localized spatial distribution.[33] As a result, the hybridized surface band changes to the Rashba-type spin splitting band structures. In the TI films, there is a breaking of inversion symmetry; the surface states have spin-momentum locking and no spin degeneracy, so that each independent surface state would show experimentally weak Rashba-type spin splitting. In other words, with the suppression of hybridization in ultrathin TI films, as shown in our results, a clear Dirac band localized at the top surface can be obtained.

To supplement the transport properties of gapless surface states of 3 QL Bi_2Se_3/graphene heterostructures, we measured the temperature-dependent resistance (RT) and magnetic conductance (MC) using a physical property measurement system (PPMS), as shown in Figure 4. First, we measured for the 20 QL Bi_2Se_3 film on a SiO_2 substrate to verify the typical transport of Bi_2Se_3 films, as shown in Supporting Information 8. By fitting with the Hikami−Larkin−Nagaoka (HLN) equation, the α value and quantum coherence length l_φ were determined to be −0.43 and 130 nm at 2 K. As the temperature increases, the α value and l_φ value decrease gradually to −0.12 and 20 nm at 80 K.[35] The decrease in the α value is caused by thermal interference with respect to the metallic state of the Bi_2Se_3 film. Moreover, l_φ has a logarithmic relationship with temperature, which is consistent with other reports.[36] The RT curves of 5 QL and 3 QL Bi_2Se_3 films grown

DOI: 10.1021/acsnano.8b07012
ACS Nano 2019, 13, 3931−3939

on graphene substrates are similar to that of the 20 QL Bi_2Se_3 film on the SiO_2 substrate (Figure 4a). As the sample temperature decreases from room temperature, the resistance values for both 5 QL and 3 QL Bi_2Se_3 films grown on graphene linearly decrease to 45 and 26 K, respectively, while for both samples, these values exponentially increase to 4 K. Below 4 K, the resistances of both samples are saturated due to the defect states of the Se vacancy.[37] The 5 QL sample has a higher resistance level than the 3 QL sample, implying that the Fermi levels of graphene substrates, which we prepared on SiO_2 substrates, are different for the two samples. In addition, the slope of the 2D electron−electron interaction region of the 5 QL sample is higher than that of the 3 QL sample because of an increase in the screening effect, implying that the carrier concentration of 5 QL Bi_2Se_3/graphene is lower than that of 3 QL Bi_2Se_3/graphene.[38]

Although there is no special sign in the RT curves of the two samples, the MC curves show unusual shapes for both 5 QL and 3 QL Bi_2Se_3/graphene heterostructures, as shown in Figure 4b. The 3 QL Bi_2Se_3/graphene shows a typical weak antilocalization shape at the low-magnetic field region, while as the magnetic field increases, the sample shows the typical weak localization (WL) shape of graphene.[39] However, the MC curves for the 5 QL Bi_2Se_3/graphene at high temperatures show the typical WL shape, while at low temperatures it shows the WAL shape under 1 T (Supporting Information 9). This difference in the MC curve with the thickness of Bi_2Se_3 on graphene reflects the typical WAL curve of TIs, as was measured for 20 QL Bi_2Se_3, in which as the temperature increases, the range of the WAL decreases because of the enhanced dephasing of electron−electron and electron−phonon scattering. This result implies that the 5 QL Bi_2Se_3/graphene has a typical TI transport channel, while the 3 QL Bi_2Se_3/graphene does not have the typical transport channel because of the proximity effect caused by the graphene.

While the typical WL in thin films resulting from the hybridization effect between two surfaces has been reported under a few hundred mT, there are unusual cusps of WAL for both 5 QL and 3 QL Bi_2Se_3/graphene heterostructures, as shown in Figure 4b. Generally, graphene shows WL curves and can exhibit WAL in very strict conditions, in which the electron dephasing time is small enough compared with the elastic inter- and intravalley scattering times; *i.e.*, graphene should be almost defect-free.[40,41] Because we used commercial graphene grown by the CVD method as a substrate in this measurement, which shows a typical WL shape, these cusps of WAL result from the transport channel of Bi_2Se_3 in the heterostructures. For these reasons, we tried to fit the whole curves under 0.2 T considering both WAL from the Bi_2Se_3 and WL from the graphene layer using the simplified HLN equation, as we fitted WAL of 20 QL Bi_2Se_3 films in Supporting Information 8 and the general equation for the WL of graphene described by McCann.[42] Detailed equations and fitted parameters including the scattering in graphene are shown in Supporting Information 10. Through the fitting process, we fitted the WAL and WL separately and obtained reasonable values of α and l_φ of the WAL of Bi_2Se_3 film. Prefactor α was found to be 0.18 in both 3 QL Bi_2Se_3/graphene and 5 QL Bi_2Se_3/graphene films, which is lower than the ideal values of 0.5 for surface transport channel of TI films. Lower values of prefactor α have been reported in ultrathin films and disordered systems with low conductivity.[43] The phase coherence lengths, however, were found to have very high values of 534 and 269 nm for 3 QL Bi_2Se_3/graphene and 5 QL Bi_2Se_3/graphene, respectively. The obtained l_φ values are even higher than that of the 20 QL Bi_2Se_3 film.

These are unusual cases because, in general, the phase coherence length in thinner films is shorter than that in thicker films for two main reasons: one is the single-channel effect resulting from strong coupling between the surface channels and conducting bulk states, and the other is the reducing Berry phase, related to the hybridization of top/bottom surfaces.[44] In our thin films, as shown in the ARPES data, the hybridization is sufficiently suppressed to induce the bandgap closing of the surface state. In addition, considering that the parabolic trend from the bulk carrier is suppressed in 3 QL Bi_2Se_3/graphene, the coupling of surface channels and conducting bulk states is reduced to cause thickness independency of the phase coherence length.[29] Thus, we conclude that the large phase coherence length of this unusual cusp is more strong evidence for a gapless topological surface state, which is consistent with the ARPES data.

The phase coherence length of Bi_2Se_3 we extracted in Bi_2Se_3/graphene heterostructures is even higher than the reported values for thin Bi_2Se_3 films, as shown in Table 1. The phase coherence length is related to the spin-flip and electron scattering, which is affected by realistic challenges such as crystalline quality, magnetic/nonmagnetic impurities, grain size, and ripples. Using a van der Waals material as a substrate, the crystalline quality improves and the film has a longer coherence length because of the increase in the mobility.[45,46] As we determined above, the Bi_2Se_3 film with a graphene substrate can have better crystalline quality and gapless Dirac states, so that the film has a much longer coherence length. As the coherence length increases, the distance over which quantum information can be transported also increases, making Bi_2Se_3/graphene heterostructures a fascinating platform for transport channels with a quantum phase, such as spins in spintronics beyond electronic devices, Cooper pairs in Josephson junctions, and Majorana fermions in superconducting junctions.

Table 1. Comparison of Phase Coherence Length with Various Sample Structures

sample structure	film thickness (QLs)	phase coherence length (nm)
Bi_2Se_3/graphene (this work)	3	534
Bi_2Se_3 on c-sapphire[16]	3 (10)	~250 (~750)
Bi_2Se_3/MoS_2 on c-sapphire[45]	20	613
Bi_2Se_3 on h-BN[46]	10	225
Al_2O_3/Bi_2Se_3/YIG[48]	20	~120
Al-passivated Bi_2Se_3 on Si(111)[49]	8	~55

CONCLUSIONS

We studied the gapless topological surface states of strained 3 QL Bi_2Se_3/graphene heterostructures observed by ARPES both computationally and experimentally. We found that compressive strain in the out-of-plane direction with graphene reduces the bandgap of the surface state of Bi_2Se_3 films. The band bending at the interface, moreover, leads to localization of the wave function of surface states and prevents the overlap of two surface states, so that the clear surface states with the closed bandgap remains to be found in ARPES. As a result, we

DOI: 10.1021/acsnano.8b07012
ACS Nano 2019, 13, 3931−3939

found that the 3 QL Bi_2Se_3/graphene heterostructure has two independent transport channels for graphene and a robust topological surface state, which results in an unusually sharp WAL cusp in the MC curves with long coherence length, which is related to the improved crystalline quality resulting from the graphene substrate and recovering of helical spin structure because of the suppression of hybridization of surface states. Therefore, we suggest that the strain and the band bending effect in TI/non-TI heterostructures may be a feasible way to engineer topological surface states beyond the physical and topological thickness limit, *i.e.*, in the heterostructure, we can not only modulate the surface band structure and its spatial distribution but also suggest practical platforms for spin and quantum devices.

METHODS

ARPES Measurement. 3−6 QL Bi_2Se_3 films were grown on epi-graphene on SiC substrate in an evaporation cell in a vacuum chamber under a pressure of 5×10^{-9} Torr. The detailed process is reported in our previous work.[24] We measured the ARPES spectrum using the synchrotron light sources of the Pohang Accelerator Laboratory (PAL) 4A1-μARPES beamline. The photoelectrons were detected by a Scienta SES-4000 electron energy analyzer at a pressure of 5×10^{-11} Torr. Energy and momentum resolutions were better than 20 meV and 0.02 $Å^{-1}$, respectively. The photon beam size was <100 μm, and data were collected at 50−100 K. 3−∼6 QL data were measured at a photon energy of 48 eV. The 2 QL and 5 QL data were measured at a photon energy of 21.22 eV (He 1).

Simulation. We calculated the surface band structure of Bi_2Se_3 films with/without monolayer graphene using the Vienna *ab initio* simulation package (VASP) PAW−PBE with van der Waals interaction (vdW-DF2(Grimme)). The Brillouin zone is sampled by a Γ-centered grid of 15 × 15 × 1. The cutoff energy is −400 eV. For all of the results, SOC is taken into consideration.

SAXS and XPS. To investigate the strain in Bi_2Se_3 films on graphene as a function of film thickness, we used GISAXS with synchrotron radiation at the 3C beamline of the PAL using a two-dimensional (2D) CCD detector (Rayonix LlC., MarCCD-165). The incidence angle of 0.2°, which is close to the critical angle, was selected to achieve the complete penetration of X-rays into the Bi_2Se_3 thin film, and monochromatic X-ray radiation with a wavelength of 1.54 Å was utilized for the beam source.

To verify the strength of spin−orbit coupling of Bi_2Se_3 films with graphene, we measured HR-XPS with a monochromatic Al Kα source (1486.6 eV) run at 15 kV and 1.67 mA. To suppress surface oxidation, we used an *in situ* transfer vessel to carry samples from the growth chamber to the XPS intro chamber.

PPMS. To measure the transport properties of Bi_2Se_3/graphene heterostructures, we used PPMS with a Keithley Series 2400 source meter and nanovoltmeter unit instruments. We used the four-point method with a wide and long transport channel (W = 50 μm, L = 1 mm), which is the same geometry we used in our previous works.[47] The range of temperature was from 2 to 300 K, and the magnetic field was up to 9 T.

ASSOCIATED CONTENT

Supporting Information

The Supporting Information is available free of charge on the ACS Publications website at DOI: 10.1021/acsnano.8b07012.

Sample confirmation using XRR, AFM, TEM, and XRD; thickness-dependent ARPES data; work function measured by UPS; calculated spatial distribution including Bi_2Se_3 and Bi_2Se_3/graphene; strain-dependent band structure of Bi_2Se_3/graphene; MC curves of 20 QL Bi_2Se_3, temperature-dependent MC of 3 QL and 5 QL Bi_2Se_3/graphene; detailed fitting parameters of 3 QL and 5 QL Bi_2Se_3/graphene (PDF)

AUTHOR INFORMATION

Corresponding Author

*Tel: +82 2 2123 5610. E-mail: mh.cho@yonsei.ac.kr.

ORCID

Keun Su Kim: 0000-0002-7033-1177
Young-Kyun Kwon: 0000-0001-6027-8408
Jeong Won Kim: 0000-0002-5881-9911
Mann-Ho Cho: 0000-0002-5621-3676

Notes

The authors declare no competing financial interest.

ACKNOWLEDGMENTS

This work was supported by the National Research Foundation of Korea (NRF) grant funded by the Korea government (MSIP) (Grant No. 2018R1A2A1A05023214) and the SRC program (vdWMRC Center, Grant No. 2017R1A5A1014862) by Samsung Research Funding Center of Samsung Electronics under Project No. SRFC-MA1502-01. We thank Hee-Suk Chung at the Korea Basic Science Institute for technical assistance with STEM, Byeong-Gyu Park at the Pohang Accelerator Laboratory for technical assistance with ARPES, and Korea Institute for Advanced Study for providing computing resources (KIAS Center for Advanced Computation Linux Cluster System).

REFERENCES

(1) Moore, J. E. The Birth of Topological Insulators. *Nature* **2010**, *464*, 194−198.

(2) Hasan, M. Z.; Kane, C. L. Colloquium: Topological Insulators. *Rev. Mod. Phys.* **2010**, *82*, 3045−3067.

(3) Hsieh, D.; Xia, Y.; Qian, D.; Wray, L.; Dil, J. H.; Meier, F.; Osterwalder, J.; Patthey, L.; Checkelsky, J. G.; Ong, N. P.; Fedorov, A. V.; Lin, H.; Bansil, A.; Grauer, D.; Hor, Y. S.; Cava, R. J.; Hasan, M. Z. A Tunable Topological Insulator in the Spin Helical Dirac Transport Regime. *Nature* **2009**, *460*, 1101−U59.

(4) Burkov, A. A.; Hawthorn, D. G. Spin and Charge Transport on the Surface of a Topological Insulator. *Phys. Rev. Lett.* **2010**, *105*, 066802.

(5) Analytis, J. G.; McDonald, R. D.; Riggs, S. C.; Chu, J. H.; Boebinger, G. S.; Fisher, I. R. Two-Dimensional Surface State in the Quantum Limit of a Topological Insulator. *Nat. Phys.* **2010**, *6*, 960−964.

(6) Shan, W. Y.; Lu, H. Z.; Shen, S. Q. Effective Continuous Model for Surface States and Thin Films of Three-Dimensional Topological Insulators. *New J. Phys.* **2010**, *12*, 043048.

(7) Zhang, Y.; He, K.; Chang, C. Z.; Song, C. L.; Wang, L. L.; Chen, X.; Jia, J. F.; Fang, Z.; Dai, X.; Shan, W. Y.; Shen, S. Q.; Niu, Q.; Qi, X. L.; Zhang, S. C.; Ma, X. C.; Xue, Q. K. Crossover of the Three-Dimensional Topological Insulator Bi_2Se_3 to the Two-Dimensional Limit. *Nat. Phys.* **2010**, *6*, 584−588.

(8) Zhang, T.; Ha, J.; Levy, N.; Kuk, Y.; Stroscio, J. Electric-Field Tuning of the Surface Band Structure of Topological Insulator Sb_2Te_3 Thin Films. *Phys. Rev. Lett.* **2013**, *111*, 056803.

(9) Galanakis, D.; Stanescu, T. D. Electrostatic Effects and Band Bending in Doped Topological Insulators. *Phys. Rev. B: Condens. Matter Mater. Phys.* **2012**, *86*, 195311.

(10) Wu, G. F.; Chen, H.; Sun, Y.; Li, X. G.; Cui, P.; Franchini, C.; Wang, J. L.; Chen, X. Q.; Zhang, Z. Y. Tuning the Vertical Location of Helical Surface States in Topological Insulator Heterostructures *via* Dual-Proximity. *Sci. Rep.* **2013**, *3*, 1233.

(11) Zhang, Q. F.; Zhang, Z. Y.; Zhu, Z. Y.; Schwingenschlogl, U.; Cui, Y. Exotic Topological Insulator States and Topological Phase

DOI: 10.1021/acsnano.8b07012
ACS Nano 2019, 13, 3931−3939

Transitions in Sb_2Se_3-Bi_2Se_3 Heterostructures. *ACS Nano* **2012**, *6*, 2345−2352.
(12) Jin, K. H.; Yeom, H. W.; Jhi, S. H. Band Structure Engineering of Topological Insulator Heterojunctions. *Phys. Rev. B: Condens. Matter Mater. Phys.* **2016**, *93*, 075308.
(13) Lee, P.; Jin, K. H.; Sung, S. J.; Kim, J. G.; Ryu, M. T.; Park, H. M.; Jhi, S. H.; Kim, N.; Kim, Y.; Yu, S. U.; Kim, K. S.; Noh, D. Y.; Chung, J. Proximity Effect Induced Electronic Properties of Graphene on Bi_2Te_2Se. *ACS Nano* **2015**, *9*, 10861−10866.
(14) Liu, W. L.; Peng, X. Y.; Wei, X. L.; Yang, H.; Stocks, G. M.; Zhong, J. X. Surface and Substrate Induced Effects on Thin Films of the Topological Insulators Bi_2Se_3 and Bi_2Te_3. *Phys. Rev. B: Condens. Matter Mater. Phys.* **2013**, *87*, 205315.
(15) Park, B. C.; Kim, T. H.; Sim, K. I.; Kang, B.; Kim, J. W.; Cho, B.; Jeong, K. H.; Cho, M. H.; Kim, J. H. Terahertz Single Conductance Quantum and Topological Phase Transitions in Topological Insulator Bi_2Se_3 Ultrathin Films. *Nat. Commun.* **2015**, *6*, 6552.
(16) Bansal, N.; Kim, Y. S.; Brahlek, M.; Edrey, E.; Oh, S. Thickness-Independent Transport Channels in Topological Insulator Bi_2Se_3 Thin Films. *Phys. Rev. Lett.* **2012**, *109*, 116804.
(17) Kim, T. H.; Baeck, J. H.; Choi, H.; Jeong, K. H.; Cho, M. H.; Kim, B. C.; Jeong, K. T. Phase Transformation of Alternately Layered Bi/Se Structures to Well-Ordered Single Crystalline Bi_2Se_3 Structures by a Self-Organized Ordering Process. *J. Phys. Chem. C* **2012**, *116*, 3737−3746.
(18) Neupane, M.; Richardella, A.; Sanchez-Barriga, J.; Xu, S.; Alidoust, N.; Belopolski, I.; Liu, C.; Bian, G.; Zhang, D. M.; Marchenko, D.; Varykhalov, A.; Rader, O.; Leandersson, M.; Balasubramanian, T.; Chang, T. R.; Jeng, H. T.; Basak, S.; Lin, H.; Bansil, A.; Samarth, N.; Hasan, M. Z. Observation of Quantum-Tunnelling-Modulated Spin Texture in Ultrathin Topological Insulator Bi_2Se_3 Films. *Nat. Commun.* **2014**, *5*, 3841.
(19) Landolt, G.; Schreyeck, S.; Eremeev, S. V.; Slomski, B.; Muff, S.; Osterwalder, J.; Chulkov, E. V.; Gould, C.; Karczewski, G.; Brunner, K.; Buhmann, H.; Molenkamp, L. W.; Dil, J. H. Spin Texture of Bi_2Se_3 Thin Films in the Quantum Tunneling Limit. *Phys. Rev. Lett.* **2014**, *112*, 057601.
(20) Sakamoto, Y.; Hirahara, T.; Miyazaki, H.; Kimura, S.; Hasegawa, S. Spectroscopic Evidence of a Topological Quantum Phase Transition in Ultrathin Bi_2Se_3 Films. *Phys. Rev. B: Condens. Matter Mater. Phys.* **2010**, *81*, 165432.
(21) Tsipas, P.; Xenogiannopoulou, E.; Kassavetis, S.; Tsoutsou, D.; Golias, E.; Bazioti, C.; Dimitrakopulos, G. P.; Komninou, P.; Liang, H.; Caymax, M.; Dimoulas, A. Observation of Surface Dirac Cone in High-Quality Ultrathin Epitaxial Bi_2Se_3 Topological Insulator on AlN(0001) Dielectric. *ACS Nano* **2014**, *8*, 6614−6619.
(22) Walter, A. L.; Bostwick, A.; Speck, F.; Ostler, M.; Kim, K. S.; Chang, Y. J.; Moreschini, L.; Innocenti, D.; Seyller, T.; Horn, K.; Rotenberg, E. Small Scale Rotational Disorder Observed in Epitaxial Graphene on SiC(0001). *New J. Phys.* **2013**, *15*, 023019.
(23) Tarakina, N. V.; Schreyeck, S.; Borzenko, T.; Schumacher, C.; Karczewski, G.; Brunner, K.; Gould, C.; Buhmann, H.; Molenkamp, L. W. Comparative Study of the Microstructure of Bi_2Se_3 Thin Films Grown on Si(111) and InP(111) Substrates. *Cryst. Growth Des.* **2012**, *12*, 1913−1918.
(24) Kim, T. H.; Jeong, K.; Park, B. C.; Choi, H.; Park, S. H.; Jung, S.; Park, J.; Jeong, K. H.; Kim, J. W.; Kim, J. H.; Cho, M. H. Tuning the Fermi Level with Topological Phase Transition by Internal Strain in a Topological Insulator Bi_2Se_3 Thin Film. *Nanoscale* **2016**, *8*, 741−751.
(25) Liu, W. L.; Peng, X. Y.; Tang, C.; Sun, L. Z.; Zhang, K. W.; Zhong, J. X. Anisotropic Interactions and Strain-Induced Topological Phase Transition in Sb_2Se_3 and Bi_2Se_3. *Phys. Rev. B: Condens. Matter Mater. Phys.* **2011**, *84*, 245105.
(26) Liu, Y.; Li, Y. Y.; Rajput, S.; Gilks, D.; Lari, L.; Galindo, P. L.; Weinert, M.; Lazarov, V. K.; Li, L. Tuning Dirac States by Strain in the Topological Insulator Bi_2Se_3. *Nat. Phys.* **2014**, *10*, 294−299.
(27) Young, S. M.; Chowdhury, S.; Walter, E. J.; Mele, E. J.; Kane, C. L.; Rappe, A. M. Theoretical Investigation of the Evolution of the Topological Phase of Bi_2Se_3 under Mechanical Strain. *Phys. Rev. B: Condens. Matter Mater. Phys.* **2011**, *84*, 085106.
(28) Thuler, M. R.; Benbow, R. L.; Hurych, Z. Synchrotron-Radiation Photoemission-Study of the V-VI Layered Compounds Bi_2Te_3, Bi_2Se_3, Sb_2Te_3 and Sb_2Te_2Se. *Chem. Phys.* **1982**, *71*, 265−270.
(29) Kim, N.; Lee, P.; Kim, Y.; Kim, J. S.; Kim, Y.; Noh, D. Y.; Yu, S. U.; Chung, J.; Kim, K. S. Persistent Topological Surface State at the Interface of Bi_2Se_3 Film Grown on Patterned Graphene. *ACS Nano* **2014**, *8*, 1154−1160.
(30) Suh, J.; Fu, D. Y.; Liu, X. Y.; Furdyna, J. K.; Yu, K. M.; Walukiewicz, W.; Wu, J. Q. Fermi-Level Stabilization in the Topological Insulators Bi_2Se_3 and Bi_2Te_3: Origin of the Surface Electron Gas. *Phys. Rev. B: Condens. Matter Mater. Phys.* **2014**, *89*, 115307.
(31) Xu, K.; Zeng, C. F.; Zhang, Q.; Yan, R. S.; Ye, P. D.; Wang, K.; Seabaugh, A. C.; Xing, H. G.; Suehle, J. S.; Richter, C. A.; Gundlach, D. J.; Nguyen, N. V. Direct Measurement of Dirac Point Energy at the Graphene/Oxide Interface. *Nano Lett.* **2013**, *13*, 131−136.
(32) Kim, S.; Ihm, J.; Choi, H. J.; Son, Y. W. Origin of Anomalous Electronic Structures of Epitaxial Graphene on Silicon Carbide. *Phys. Rev. Lett.* **2008**, *100*, 176802.
(33) Park, K.; De Beule, C.; Partoens, B. The Ageing Effect in Topological Insulators: Evolution of the Surface Electronic Structure of Bi_2Se_3 upon K Adsorption. *New J. Phys.* **2013**, *15*, 113031.
(34) Pertsova, A.; Canali, C. M. Probing the Wavefunction of the Surface States in Bi_2Se_3 Topological Insulator: a Realistic Tight-Binding Approach. *New J. Phys.* **2014**, *16*, 063022.
(35) Hikami, S.; Larkin, A. I.; Nagaoka, Y. Spin-Orbit Interaction and Magnetoresistance in the Two Dimensional Random System. *Prog. Theor. Phys.* **1980**, *63*, 707−710.
(36) Gopal, R. K.; Singh, S.; Mandal, A.; Sarkar, J.; Mitra, C. Topological Delocalization and Tuning of Surface Channel Separation in Bi_2Se_2Te Topological Insulator Thin Films. *Sci. Rep.* **2017**, *7*, 4924.
(37) He, L.; Xiu, F. X.; Yu, X. X.; Teague, M.; Jiang, W. J.; Fan, Y. B.; Kou, X. F.; Lang, M. R.; Wang, Y.; Huang, G.; Yeh, N. C.; Wang, K. L. Surface-Dominated Conduction in a 6 nm thick Bi_2Se_3 Thin Film. *Nano Lett.* **2012**, *12*, 1486−1490.
(38) Kozikov, A. A.; Savchenko, A. K.; Narozhny, B. N.; Shytov, A. V. Electron-Electron Interactions in the Conductivity of Graphene. *Phys. Rev. B: Condens. Matter Mater. Phys.* **2010**, *82*, 075424.
(39) Tikhonenko, F. V.; Horsell, D. W.; Gorbachev, R. V.; Savchenko, A. K. Weak Localization in Graphene Flakes. *Phys. Rev. Lett.* **2008**, *100*, 056802.
(40) Lu, H. Z.; Shi, J. R.; Shen, S. Q. Competition between Weak Localization and Antilocalization in Topological Surface States. *Phys. Rev. Lett.* **2011**, *107*, 076801.
(41) Tikhonenko, F. V.; Kozikov, A. A.; Savchenko, A. K.; Gorbachev, R. V. Transition between Electron Localization and Antilocalization in Graphene. *Phys. Rev. Lett.* **2009**, *103*, 226801.
(42) McCann, E.; Kechedzhi, K.; Fal'ko, V. I.; Suzuura, H.; Ando, T.; Altshuler, B. L. Weak-Localization Magnetoresistance and Valley Symmetry in Graphene. *Phys. Rev. Lett.* **2006**, *97*, 146805.
(43) Liao, J.; Ou, Y. B.; Feng, X.; Yang, S.; Lin, C. J.; Yang, W. M.; Wu, K. H.; He, K.; Ma, X. C.; Xue, Q. K.; Li, Y. Q. Observation of Anderson Localization in Ultrathin Films of Three-Dimensional Topological Insulators. *Phys. Rev. Lett.* **2015**, *114*, 216601.
(44) Kim, Y. S.; Brahlek, M.; Bansal, N.; Edrey, E.; Kapilevich, G. A.; Iida, K.; Tanimura, M.; Horibe, Y.; Cheong, S. W.; Oh, S. Thickness-Dependent Bulk Properties and Weak Antilocalization Effect in Topological Insulator Bi_2Se_3. *Phys. Rev. B: Condens. Matter Mater. Phys.* **2011**, *84*, 073109.
(45) Chen, K. H. M.; Lin, H. Y.; Yang, S. R.; Cheng, C. K.; Zhang, X. Q.; Cheng, C. M.; Lee, S. F.; Hsu, C. H.; Lee, Y. H.; Hong, M.; Kwo, J. Van der Waals Epitaxy of Topological Insulator Bi_2Se_3 on Single Layer Transition Metal Dichalcogenide MoS_2. *Appl. Phys. Lett.* **2017**, *111*, 083106.

DOI: 10.1021/acsnano.8b07012
ACS Nano 2019, 13, 3931−3939

(46) Park, J. Y.; Lee, G. H.; Jo, J.; Cheng, A. K.; Yoon, H.; Watanabe, K.; Taniguchi, T.; Kim, M.; Kim, P.; Yi, G. C. Molecular Beam Epitaxial Growth and Electronic Transport Properties of High Quality Topological Insulator Bi_2Se_3 Thin Films on Hexagonal Boron Nitride. *2D Mater.* **2016**, *3*, 035029.
(47) Park, S. H.; Chae, J.; Jeong, K. S.; Kim, T. H.; Choi, H.; Cho, M. H.; Hwang, I.; Bae, M. H.; Kang, C. Reversible Fermi Level Tuning of a Sb_2Te_3 Topological Insulator by Structural Deformation. *Nano Lett.* **2015**, *15*, 3820−3826.
(48) Jiang, Z. L.; Katmis, F.; Tang, C.; Wei, P.; Moodera, J. S.; Shi, J. A Comparative Transport Study of Bi_2Se_3 and Bi_2Se_3/Yttrium Iron Garnet. *Appl. Phys. Lett.* **2014**, *104*, 222409.
(49) Lang, M. R.; He, L.; Xiu, F. X.; Yu, X. X.; Tang, J. S.; Wang, Y.; Kou, X. F.; Jiang, W. J.; Fedorov, A. V.; Wang, K. L. Revelation of Topological Surface States in Bi_2Se_3 Thin Films by *In Situ* Al Passivation. *ACS Nano* **2012**, *6*, 295−302.

DOI: 10.1021/acsnano.8b07012
ACS Nano 2019, 13, 3931−3939